Biochimie 94 (2012) 628–636

Contents lists available at SciVerse ScienceDirect

Biochimie

journal homepage: www.elsevier.com/locate/biochi

Research paper

Self assembly of human septin 2 into amyloid filaments

Julio Cesar Pissuti Damalio[a], Wanius Garcia[b], Joci Neuby Alves Macêdo[a], Ivo de Almeida Marques[a], José M. Andreu[c], Rafael Giraldo[c], Richard Charles Garratt[a], Ana Paula Ulian Araújo[a,*]

[a] Centro de Biotecnologia Molecular Estrutural, Instituto de Física de São Carlos (IFSC), Universidade de São Paulo (USP), Av. Trabalhador Sãocarlense, 400, 13560-970 São Carlos, SP, Brazil
[b] Centro de Ciências Naturais e Humanas (CCNH), Universidade Federal do ABC (UFABC), Santa Adélia, 148, Santo André, SP, Brazil
[c] Centro de Investigaciones Biológicas-CSIC, Madrid, Spain

ARTICLE INFO

Article history:
Received 18 May 2011
Accepted 15 September 2011
Available online 28 September 2011

Keywords:
GTPase domain
Aggregates
Amyloid
Neurodegenerative diseases
Septin

ABSTRACT

Septins are a conserved group of GTP-binding proteins that form hetero-oligomeric complexes which assemble into filaments. These are essential for septin function, including their role in cytokinesis, cell division, exocytosis and membrane trafficking. Septin 2 (SEPT2) is a member of the septin family and has been associated with neurofibrillary tangles and other pathological features of senile plaques in Alzheimer's disease. An *in silico* analysis of the amino acid sequence of SEPT2 identified regions with a significant tendency to aggregate and/or form amyloid. These were all observed within the GTP-binding domain. This was consistent with the experimental identification of a structure rich in β-sheet during temperature induced unfolding transitions observed for both the full length protein and the GTP-binding domain alone. This intermediate state is characterized by irreversible aggregation and has the ability to bind Thioflavin-T, suggesting its amyloid nature. Under electron microscopy, fibers extending for several micrometers in length could be visualized. The results shown in this study support the hypothesis that single septins, when present in excess or with unbalanced stoichiometries, may be unstable and assemble into amyloid-like structures.

1. Introduction

The septins are members of a conserved group of GTP-binding proteins, originally discovered in yeast as being required for the completion of the cell cycle [1]. Septins have been identified in all animals and fungi [2]. In mammals they are involved in a variety of cellular phenomena, such as microtubule regulation [3,4], vesicle trafficking [5], the assembly of scaffolding platforms [6], actin dynamics [7], exocytosis [8], apoptosis [9], DNA repair [10] and mechanical stability [11–13].

All members of the septin family can be divided into three domains: a variable N-terminal domain, a GTP-binding domain and a C-terminal region, which generally includes sequences with the potential to assemble as a coiled-coil [14]. In addition, some septins have a polybasic region between the N-terminal and GTP-binding domains, which is responsible for lipid interaction [15]. Both the binding of GTP and its hydrolysis have been experimentally demonstrated for several septins *in vitro* [2,16–18].

Septins can assemble into high-order hetero-filaments, including two or more members of the family, *in vivo* and *in vitro*. These hetero-filaments were isolated from *Drosophila melanogaster* [19] and fungi [20], and shown to have a width of about 7–9 nm and a variable length. Hetero-filaments were also identified in the case of the *Caenorhabditis elegans* septins UNC-59 and UNC-61 [21]. Moreover, a complex of recombinant *Saccharomyces cerevisiae* septins, Cdc3, Cdc10, Cdc11 and Cdc12, forms an elongated linear octamer composed of two copies of each individual septin which subsequently polymerize to form filaments [22]. Recently, Sirajuddin et al. solved the crystal structures of both the human SEPT2 GTP-binding domain alone and the hetero-trimeric complex of SEPT2–SEPT6–SEPT7 [23]. In both cases the crystal lattice leads to the formation of filaments. In addiction, members of the same group can replace each other in the specific position along the heterofilament [24].

Although the formation of hetero-filaments by septins and their associated functions is relatively well established, information concerning the existence and physiological role of homo-filaments is puzzling. The first report of filaments formed by a single septin was that for *Xenopus laevis* SEPT2. The authors described homo-filaments of 20 nm in width when the component monomers were bound to GTP but not to GDP [25]. This observation has been

* Corresponding author. Tel.: +55 16 33739875; fax: +55 1633715381.
E-mail address: anapaula@ifsc.usp.br (A.P. Ulian Araújo).

0300-9084/$ – see front matter © 2011 Elsevier Masson SAS. All rights reserved.
doi:10.1016/j.biochi.2011.09.014

subsequently questioned, leaving some doubt about the relevance of homo-filaments in the case of *Xenopus* septins [26]. However, 20–40 nm wide homo-filaments have also been reported for human SEPT2 in both the GTP- and GDP-bound states [18]. The question of the existence of homo-filaments is therefore unsettled and has been complicated by the observation of homo-filaments of human SEPT4, which are believed to be amyloid fibers with no physiological relevance [27].

SEPT2 is essential for cytokinesis, being located near the contractile ring from anaphase to telophase and finally condensing into the midbody [7]. It has a wide tissue distribution and specifically in the brain has been observed to co-localize with GLAST, an astrocyte glutamate transporter [28]. Based on this data SEPT2 has been suggested to play a role in signal transmission in the cerebellum [28]. Besides its physiological roles, SEPT2 has also been implicated in several pathologies including leukemia and lymphoma [29], renal cell carcinoma [30], brain tumors [31,32] and systemic lupus erythematosus [33]. Moreover, SEPT2 together with SEPT1 and SEPT4 (all of which are acidic proteins) have been seen to accumulate in neurofibrillary tangles (NFTs) in Alzheimer's disease [34] where they co-localize with the basic microtubule-associated protein tau. So far, however, the role of septins in NFT formation and the possible mechanisms of self-aggregation of septins in neurodegenerative disorders still remain unclear.

A wide range of human pathologies are associated with uncontrolled protein misfolding, leading to the conversion of polypeptide chains from their soluble globular states into well-organized fibrillar aggregates rich in β-sheet structure [35,36]. Amyloid formation is the hallmark of medically related disorders, such as Alzheimer disease, and more than 40 human related diseases have been described, each having a distinct clinical profile and each associated with the aggregation of a single dominant protein [37].

With the aim of shedding some light upon this issue, the present study uses a biophysical approach to investigate the stability and aggregation of SEPT2. Our results show that both SEPT2 and its GTP-binding domain (SEPT2G) are dimeric in solution, but they have the tendency to rapidly aggregate at physiological temperatures. These aggregates have the ability to bind Thioflavin-T, suggesting that they are amyloids and providing the first insight on the mechanisms that cause the formation of the aggregates associated with neurodegenerative diseases.

2. Material and methods

2.1. Materials and reagents

The bacterial expression vector pET28a(+) and Ni-NTA resin were purchased from Novagen. Restriction endonucleases, isopropyl-β-D-thiogalactopyranoside, kanamycin, T4 DNA ligase and *Taq* Polymerase were obtained from Invitrogen. The Superdex-200 column 10/30 and native gels for electrophoresis [8–25% (w/v) gradient polyacrylamide] were purchased from Amersham Pharmacia Biotech (GE-Healthcare). Guanosine-5′-diphosphate (GDP), protein standard markers and ThT (Thioflavin-T) were purchased from Sigma. All other chemical products used were obtained from Sigma and/or GE-Healthcare.

2.2. In silico analysis

Essentially, protein aggregation is a self-assembly of identical molecules [38], and these aggregates can be classified as either ordered or disordered, on the basis of their intimate structural features [39]. There is evidence that local unfolding events can cause the aggregation of normally globular proteins into well-organized fibrils [40]. In order to identify possible regions presenting a high aggregation probability in SEPT2, we used the *in silico* analysis programs TANGO, WALTZ and ZYGGREGATOR. TANGO is a statistical mechanics algorithm which predicts protein aggregation, based on the physico-chemical principles of β-sheet formation [41,42]. WALTZ and ZYGGREGATOR are algorithms including additional thermodynamic information in the prediction of regions with a high probability to form amyloid sequences [43,44]. The amino acid sequence of SEPT2 was submitted to these prediction programs using servers based at http://tango.crg.es/ and http://waltz.switchlab.org/, using default parameters. Additionally, the major isoforms of all 13 human septin sequences were also analyzed with WALTZ in order to compare their predicted amyloidogenic regions.

2.3. Plasmid construction and proteins expression

Based on the results of the sequence analysis, which suggested the presence of aggregation prone sequences within the GTP-binding domain, a construct was designed corresponding to a truncated SEPT2 protein covering this region of the molecule (SEPT2G, residues 34–308). The cDNA corresponding to SEPT2 (residues 1–361) and its GTP-binding domain (SEPT2G) were amplified using the polymerase chain reaction performed in a Mastercycler thermocycler (Eppendorf), using a fetal brain cDNA library (Gibco BRL) as template. Amplification products were purified and cloned into the pET28a(+) expression vector, using *Nde*I and *Xho*I restriction sites. The recombinant plasmids were transformed into *Escherichia coli* DH5α for propagation and plasmid extraction purposes. These were named pSEPT2 and pSEPT2G and produced their respective products fused to an N-terminal His-tag. All plasmids were sequenced by the dideoxy chain method [45] using an ABI Prism 377 automated DNA sequencer (Perkin–Elmer) following the protocol of the manufacturer.

The expression plasmids were used to transform the *E. coli* host strain BL21(DE3). A total of 500 μL of an overnight culture of *E. coli* BL21(DE3) harboring the pSEPT2 plasmid were inoculated into 500 mL of fresh LB medium containing kanamycin (50 μg/mL). The culture was grown whilst shaking at 37 °C to mid log phase ($O.D._{600nm} = 0.6$) and subsequently induced with IPTG at a final concentration of 0.4 mM followed by incubation for 10 h at 18 °C.

After centrifugation, the pelleted cells were re-suspended in 25 mM Tris–HCl pH 7.8 buffer, containing 100 μM GDP and 10% glycerol. The cells were disrupted by the addition of 0.1 mg/mL lysozyme for 30 min at 4 °C, followed by sonication. The suspension was then centrifuged at 18,000 g for 20 min at 4 °C, and the pellet and supernatant were analyzed by SDS-PAGE to check the solubility of the recombinant protein. The supernatant containing the recombinant SEPT2 was loaded onto a nickel-affinity column equilibrated with the same buffer. After the unbound proteins were eliminated by exhaustive washing, SEPT2 was eluted by increasing concentrations of imidazole up to 300 mM.

The resulting SEPT2 was then loaded onto a Superdex-200 10/300 GL column (GE-Healthcare) pre-equilibrated with 25 mM Tris–HCl pH 7.8 buffer, containing 10% glycerol and driven by an Åkta purifier. The elution was carried out in the same buffer, at 4 °C and fractions analyzed by means of 15% SDS-PAGE. Protein elution was monitored by absorbance at 280 nm. The elution volumes of standard proteins were used to calculate the *K*av values [*K*av = (elution volume − column void volume)/(total column volume − column void volume)]. The standard proteins of known molecular weight were carbonic anhydrase (29 kDa), ovoalbumin (43 kDa), conalbumin (75 kDa), ferritin (440 kDa) and lactoglobulin (669 kDa). An identical protocol was used for the purification of SEPT2G. The protein concentration, in all cases, was determined from its absorbance at 280 nm, based on its amino acid composition [46], employing a U-2001 Hitachi UV–visible spectrophotometer.

2.4. Native gel electrophoresis

SEPT2 (20 μM) and SEPT2G (20 μM) were centrifuged at 13,000 × g for 5 min at 4 °C. Subsequently the samples were subjected to electrophoresis on an 8–25% (w/v) gradient polycrylamide gel at pH 8.8 using the Phast System (Amersham Bioscience), at 4 °C, and stained following standard protocols. Protein standards of known hydrodynamic radii (thyroglobulin, 8.5 nm; ferritin, 6.1 nm; catalase, 5.22 nm; lactate dehydrogenase, 4.4 nm; and bovine serum albumin, 3.55 nm) were subjected to electrophoresis under identical conditions. The mobilities of the individual bands of the protein standards were plotted as the retardation factors (R_f) versus the Stokes radii (R_h). The linear equation obtained from this calibration was employed to calculate the R_h of SEPT2 and SEPT2G.

2.5. Circular dichroism spectroscopy (CD)

The thermal unfolding of the recombinant proteins, SEPT2 and SEPT2G was monitored by far-UV CD spectroscopy over a wavelength range of 195–250 nm, using a J-715 Jasco spectropolarimeter equipped with a temperature controller. CD spectra were measured from samples in 0.1 cm quartz cuvettes and were the average of 16 accumulations, using a scanning speed of 100 nm min^{-1}, a spectral bandwidth of 1 nm, and a response time of 0.5 s. The protein concentration, in all cases, was approximately 10 μM in 25 mM Tris–HCl, pH 7.8 buffer containing 10% glycerol. Thermal denaturation measurements were performed by incubating the samples for 30 min at temperatures of 15 °C, 30 °C, 37 °C, 45 °C and 60 °C. CD spectra were obtained on a degree ellipticity scale and the buffer contribution was subtracted in all of the experiments. Data points were analyzed with the software Origin 7.0 and deconvolution of the spectrum was performed using the K2d algorithm (http://www.embl-heidelberg.de/~andrade/k2d/).

2.6. Right-angle light scattering

SEPT2 and SEPT2G (5 μM) in 25 mM Tris–HCl, pH 7.8 buffer containing 10% glycerol were centrifuged (16,000 × g for 10 min at 4 °C) and each sample placed in a 1 cm path length quartz cuvette in a spectrofluorimeter, model K2 ISS, equipped with a refrigerated circulator. The samples were illuminated with 350 nm light, and the scattering at the same wavelength was collected at an angle of 90°. Measurements were made at 15 °C, 30 °C, 37 °C, 45 °C and 60 °C. All intensity measurements were normalized to values between 0 and 1 (where the latter corresponds to the maximum intensity obtained at 60 °C) after subtraction of the light scattering by the buffer. Data points were analyzed with the software Origin 7.0.

2.7. Thioflavin-T fluorescence assay

Thioflavin T (ThT) is the most commonly used dye for the detection of amyloid aggregates [47,48], and it is speculated that ThT may bind in between the β-sheets of the fibril [49]. Proteins at 5 μM (in 25 mM Tris–HCl, 10% glycerol, pH 7.8 buffer) were used in this experiment to analyze the ThT binding to SEPT2 and SEPT2G. The proteins were incubated with 80 μM ThT, excited at 450 nm and the emission measured at 482 nm for a period of 90 min. Measurements were made at 15 °C, 30 °C, 37 °C, 45 °C and 60 °C. All intensity measurements were normalized to values between 0 and 1, after subtraction of the light scattering by the buffer. Data points were analyzed with the software Origin 7.0.

2.8. Electron microscopy

In order to verify the morphology of the SEPT2 aggregates, the sample (5 μM) was maintained at 37 °C for 30 min in buffer containing 25 mM Tris–HCl, 10% glycerol, pH 7.8. Samples incubated at 4 °C for 5 days were also prepared in order to decrease the rate of amyloid filament formation. Negative staining was performed as follows. Initially samples were applied to glow-discharged carbon-coated grids for 1 min. These were stained with filtered 1% uranyl acetate for 1 min, subsequently washed with a drop of the same buffer and blotted dry. Images were acquired with a transmission electron microscope Philips CM 120 or a JEOL JEM 1230, working at 80 or 100 kV.

3. Results and discussion

3.1. SEPT2 presents regions with high probability of aggregation and/or amyloid formation

It is accepted that two mechanisms appear to control the assembly of amyloid oligomers, one sequence-dependant and the other sequence-independent [50]. Obviously, the sequence-dependant mechanism is more predictable and the programs TANGO and WALTZ are very sensitive for the detection of β-sheet aggregation and amyloidogenic regions, respectively [41,43]. The TANGO results indicated four regions of SEPT2 presenting a high probability of aggregation through β-sheets, all of them within the GTP-binding domain. The sequences identified included those between residues 38 and 43 (FTLMVV), 52 and 59 (TLINSLFL), 118 and 122 (IISYI) and 146 and 153 (VHCCFYFI) (Fig. 1A). Although TANGO aims to predict β-sheet aggregation but not specifically amyloid formation, there is a good correlation between the two [41].

The program WALTZ aims to minimize the over prediction of amorphous β-aggregation compared to the regular cross-β structure characteristic of amyloid fibrils, making it more specific for the latter [51]. WALTZ also identified four regions within SEPT2 which presented a high amyloidogenic potential: the sequences between residues 118 and 123 (IISYID), 147 and 155 (HCCFYFISP), 163 and 168 (LDVAFM), 173 and 178 (NKVNIV) (Fig. 1A). Once again these regions were all restricted to the GTP-binding domain and two of the WALTZ predictions were effectively identical to those identified by TANGO, being highly suggestive that these regions have a tendency towards self-assembly and amyloid formation. The region from 118 to 123 corresponds to a helical region on the surface of the monomer whilst that from 147 to 155 maps to a buried β-strand. They are shown in red and blue in Fig. 1B and C. Furthermore, both of these regions were also identified by the independent algorithm Zyggregator. In both cases considerable structural rearrangement of the monomer would therefore be necessary in order for these particular sequences to become solvent exposed and directly participate in the cross-β spine, eventually leading to aggregation. In order to investigate this further, SEPT2 and SEPT2G were over-expressed for structural analysis.

3.2. SEPT2 and SEPTG are dimers in solution

The definition of the GTP-binding domain for SEPT2 was based on that used in a previous study of the molecular dissection of SEPT4 [52]. DNA amplifications produced fragments of 1083 and 822 bp corresponding to the coding regions of SEPT2 and SEPT2G, respectively. After induction with IPTG, *E. coli* cells harboring the appropriate expression vector produced additional bands of around 44 and 34 kDa corresponding to SEPT2 and SEPT2G, respectively. In both cases, the majority of the expressed product was soluble after cell lysis and final yields were typically 3 and 10 mg of recombinant protein/L of culture medium for SEPT2 and SEPT2G, respectively.

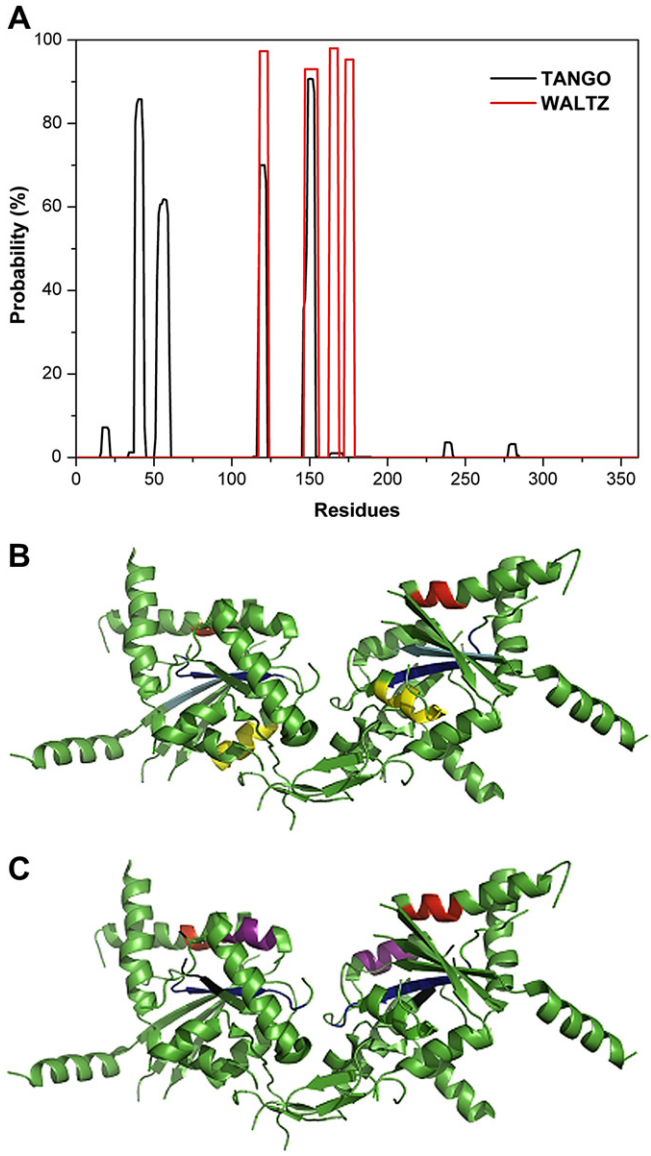

Fig. 1. *In silico* sequence analysis of SEPT2 (A). The programs TANGO and WALTZ indicate four regions with a high probability (>60%) of β-sheet aggregation and amyloid formation, respectively. (B): The 3D structure of SEPT2 (2QA5 pdb code) showing the regions predicted by TANGO: 38FTLMVV43 (cyan), 52TLINSLFL59 (yellow), 118IISYI122 (red), 146VHCCFYFI153 (blue); (C): SEPT2 showing the regions predicted by WALTZ: 118IISYID123 (red), 147HCCFYFISP155 (blue), 163LDVAFM168 (purple), 173NKVNIV178 (black). Two effectively identical regions were identified within the GTP-binding domain by both programs. (For interpretation of the references to colour in this figure legend, the reader is referred to the web version of this article.)

The recombinant proteins showed GTPase activity (data not shown), as previously reported [18].

Upon SEC, the full length SEPT2 molecule eluted as a single peak of apparent molecular weight of around 91 kDa (Fig. 2, solid line), which is consistent with a dimer, whose expected mass is 88 kDa. This is broadly supported by the results of native gel electrophoresis, which showed a major band migrating below lactate dehydrogenase (140 kDa) (Fig. 3B, lane 2). The hydrodynamic radius calculated for SEPT2 from its R_f value was 4.6 nm, corresponding a molecular weight of approximately 120 kDa, considering a spherical particle. This value is compatible with a dimer or a trimer for SEPT2 in solution under native conditions, but definitive conclusions are limited by the fact that a SEPT2 dimer would not be expected to be a spherical particle.

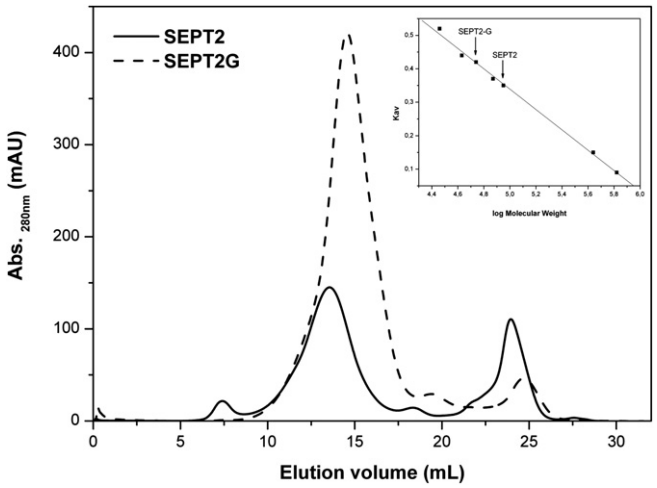

Fig. 2. Elution profile of SEPT2 and its GTP-binding domain (SEPT2G) on Size Exclusion Chromatography. Both proteins eluted as dimers in solution in the presence of GDP. Excess nucleotide corresponds to the peak observed close to fraction 25. The elution volumes of standard proteins were used to calculate *K*av values (inset). The main peak position corresponded to about 91 kDa for SEPT2 and 60 kDa for SEPT2G.

SEPT2G eluted as a single peak with an apparent molecular weight of approximately 60 kDa (Fig. 2, dotted line), consistent with a dimer, whose expected mass is 68 kDa. Furthermore, the native gel showed a major band migrating similarly to BSA (67 kDa) (Fig. 3B, lane 3). The hydrodynamic radius of SEPT2G was calculated to be 3.9 nm, corresponding to a molecular weight of 74 kDa, consistent with a dimer under native conditions. The recombinant proteins migrated with the expected molecular mass under denaturing conditions in 15% SDS-PAGE (Fig. 3A). Taken together, these data indicate that both human SEPT2 and SEPT2G are dimeric molecules in solution, agreeing with the structural results obtained for human SEPT2-315, which shows that the dimer is stabilized by interactions across the nucleotide-binding G interface [23].

3.3. *At higher temperatures SEPT2 and SEPT2G show a structural transition*

Amyloidogenic proteins are rich in β-sheet secondary structure in which the strands lie orthogonal to the fiber axis [53]. Structural transition of buried segments in protein chains into solvent-exposed β-strands is a remarkable characteristic of a number of conformational diseases [41,54–56]. Circular dichroism was therefore used to probe SEPT2 and SEPT2G in order to investigate if the dimeric structure described above is susceptible to such structural transitions. At 15 °C, the far-UV CD of both spectra exhibit two negative minima at 208 nm and 220 nm, which are characteristic of the presence of α-helical secondary structure. The deconvolution of the SEPT2G spectrum led to an estimated content of 25% α-helix, 24% β-strand and 50% turns/irregular structures. This is compatible with the data from the tridimensional structure of SEPT2-315 (2QA5 pdb code, Fig. 1), which gave values of 32% α-helix and 15% β-strand and 53% turns/irregular structures. However, it should be pointed out that the construct used in the crystallographic studies is slightly different from that described here.

On increasing the temperature, marked changes in the secondary structure of SEPT2 took place (Fig. 4A and B). Above 30 °C loss in the α-helical content can be readily observed. This can be followed by the change in the ellipticity at 220 nm, which is the dominant trough characteristic of α-helical structure. This is clearer in SEPT2G, which lacks the C-terminal coiled-coil domain, responsible for a significant percentage of the helical component in

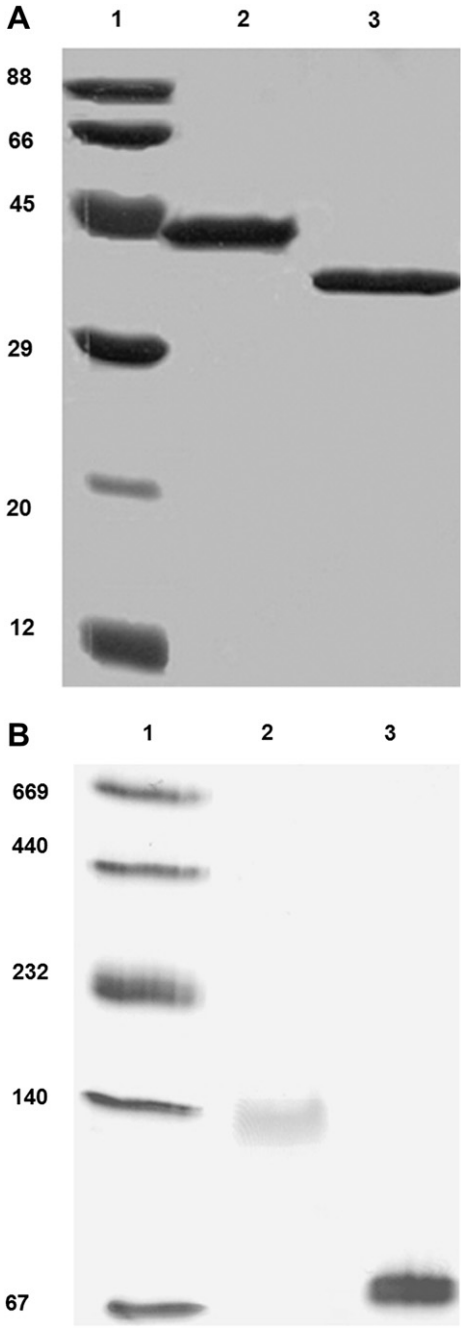

Fig. 3. A) SEPT2 profile on 15% SDS-PAGE. Lane 1: Molecular weight markers; Lane 2: SEPT2; Lane 3: SEPT2G. B) SEPT2 under Native Gel Electrophoresis (8–25%). Lane 1: Molecular weight markers; Lane 2: SEPT2; Lane 3: SEPT2G. The estimated hydrodynamic radii were 4.6 nm for SEPT2 and 3.9 nm for SEPT2G.

the case of SEPT2. At higher temperatures the spectrum acquires characteristics of β-sheet structure, with a minimum between 215 nm and 220 nm, consistent with the results of deconvolution of the spectrum measured at 45 °C, which yielded 15% α-helix, 35% β-strand and 50% turns/irregular structures. Above 60 °C, the spectrum looses overall intensity and the sample begins to precipitate.

3.4. Formation of high order particles in solution

In order to evaluate whether the heat treatment was promoting aggregation of the proteins, right-angle light scattering (RALS)

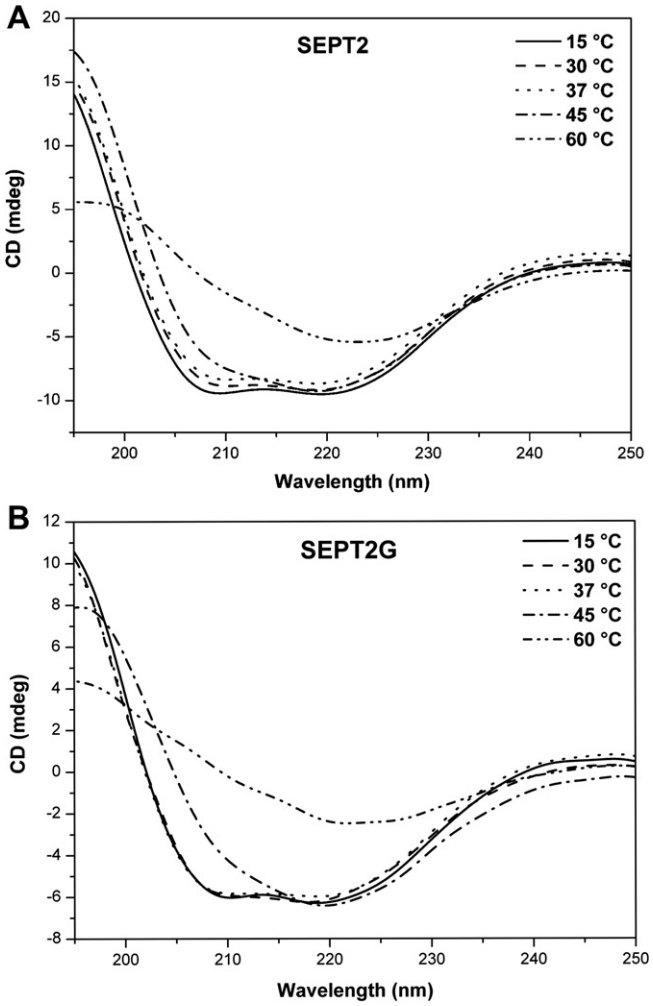

Fig. 4. Thermal unfolding of SEPT2 and SEPT2G. Circular Dichroism (CD) spectra as a function of temperature were recorded in 25 mM Tris–HCl pH 7.8, 10% Glycerol. In both cases, although no significant change to the CD spectrum could be observed from 15 °C to 30 °C, above this temperature a loss in the characteristic transitions indicating the presence of α-helix can be observed the spectral profile.

measurements were performed. Initially, SEPT2 (Fig. 5A) and SEPT2G (Fig. 5B) were measured at temperatures between 15 °C and 60 °C, and RALS was followed as a function of time. In both cases, the intensity of scattered light remained constant at 15 °C for the entire duration of the experiment, indicating that no protein aggregation was detectable under these conditions. However, in the interval from 30 °C to 60 °C the intensity of light scattering increased over time in a temperature dependent manner, reaching a maximum intensity at 60 °C. This intensity subsequently remained constant over time and there was no evidence of protein precipitation. These data suggest the temperature dependent formation of larger particles in solution. SEPT2 showed a more rapid aggregation than SEPT2G suggesting that the presence of the non-globular N- and C-terminal domains may lead to rapid amorphous aggregation.

3.5. SEPT2 and SEPT2G bind ThT

ThT exhibits enhanced fluorescence upon binding to amyloid fibrils, both *in vivo* and *in vitro* [37] and this was monitored at 482 nm in the case of SEPT2 (Fig. 6A) and SEPT2G (Fig. 6B) on incubation at the same temperatures used to study protein

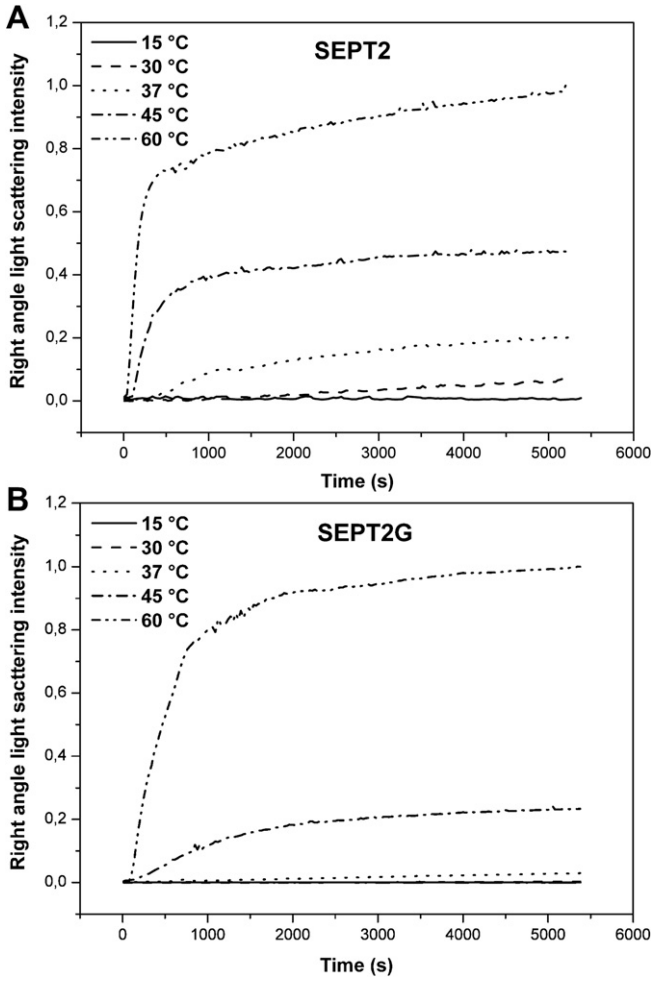

Fig. 5. Right angle light scattering of SEPT2 and SEPT2G as a function of temperature. Scattering intensity at 350 nm was measured as a function of time at each temperature for the two samples. Both proteins show a rapid aggregation at temperatures above 30 °C.

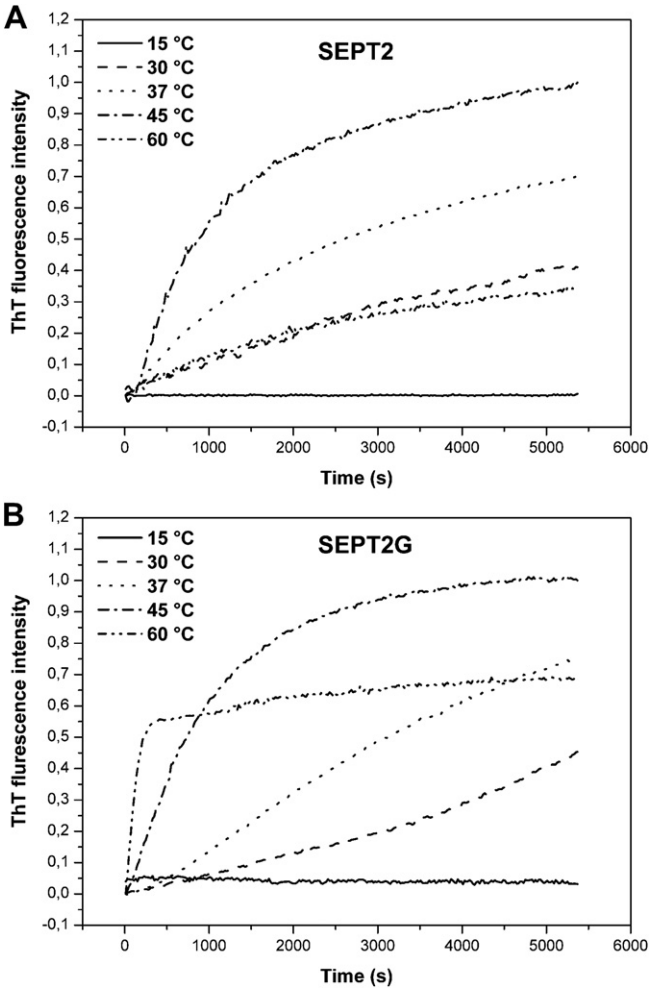

Fig. 6. ThT fluorescence emission spectra of SEPT2 and SEPT2G as a function of temperature. Fluorescence emission was monitored at 482 nm after excitation at 450 nm. In both cases, some degree of ThT binding (indicative of amyloid formation) can be observed even at 30 °C. At 45 °C the greatest degree of binding is observed, reaching a maximum after approximately 1000 s. At 60 °C a rapid increase in the fluorescence emission is observed during the first few minutes in the case of SEPT2G which is followed by a reduction in the emission intensity due to the formation of amorphous aggregates.

aggregation. The level of ThT fluorescence emission increased up to a maximum value in both cases, and this behavior was temperature dependent. In the case of the measurements made at 45 °C, the plateau could be clearly seen and was reached after approximately 1000 s. This is the temperature at which the structure rich in β-sheet, strongly suggestive of amyloid formation, is observed on thermal unfolding. Indeed, at 37 °C and 45 °C both proteins released the nucleotide, which is normally buried within the GTPase domain (Supplementary material, Figure S1). At higher temperatures (above 45 °C) there is a reduction in the maximum fluorescence intensity reached indicating an increase in the formation of amorphous aggregates rather than amyloid. Such aggregates are expected to be the result of rapid partial unfolding of the protein at higher temperatures and the consequent exposure of hydrophobic regions. These contribute to light scattering but cannot be detected by ThT fluorescence emission. Furthermore, incubation of SEPT2G with DTNB (5,5′-dithiobis,2-nitrobenzoic acid) [57] demonstrated an increase in binding as a function of temperature followed by a sharp decline above 37 °C (data not shown). This is consistent with the initial exposure of the region 147HCCFYFISP155, (which contains two of the protein's four cysteine residues) followed by its subsequent burial, coherent with the participation of this region in amyloid formation.

An interesting difference can be observed between the two constructs studied. SEPT2G shows a sharp rise in ThT fluorescence emission at 60 °C demonstrating the initial rapid formation of amyloid-like structures which subsequently becomes dominated by amorphous aggregation leading to a flattening of the curve. This behavior can be verified by comparing the corresponding curves in Figs. 5 and 6B. SEPT2 aggregation at 60 °C, on the other hand, appears to involve a greater amorphous component right from the outset. These results suggest that the GTP-binding domain is sufficient for the formation of amyloid-like structures as predicted by the results of the sequence analyses with TANGO and WALTZ. The difference in the behavior of the two constructs can be attributed to the presence of the N- and C-terminal domains in the case of SEPT2 which are not predicted to be involved in amyloid formation but could readily contribute to other forms of protein aggregation at higher temperatures.

Ideally, in order to verify the direct participation of the predicted regions in amyloid formation, mutagenesis of these sequences would be necessary. However, an exhaustive study of potential mutations using the CUPSAT algorithm [58] indicated the majority

of these to be destabilizing. Furthermore, given the possible involvement of more than one amyloidogenic region, a series of single and double mutants would be necessary in order to properly test this hypothesis. Unfortunately, these limitations would lead to considerable ambiguity when interpreting the outcome.

3.6. Amyloid like filaments are visualized by electron microscopy

To evaluate the formation of amyloid-like fibers, SEPT2 was incubated at 37 °C for 30 min (Fig. 7A). At this temperature, chosen to be below that at which SEPT2 rapidly binds ThT, the samples have the ability to form amyloid-like aggregates similar to those observed for SEPT4 [27]. It was also observed the presence of amorphous aggregates, probably due to the time and temperature that the sample was incubated. In an attempt to decrease the velocity of this process even further, SEPT2 was incubated at 4 °C for 120 h. Under these conditions we observed a small number of well-defined filaments of 20 nm in diameter and lengths of up to several micrometers (Fig. 7B). At this lower temperature the sample still bound ThT, but at a much reduced rate (in 90 min there is no detection of ThT binding), compared with 45 °C (Supplementary material, Figure S2). This strongly suggests that filament formation can occur over a wide range of temperatures but is accelerated on heating.

An overall picture emerges in which the natural tendency of the GTP-binding domain of SEPT2 to form amyloid-like aggregates is exacerbated at temperatures, which favor the partial unfolding of the protein and the appearance of β-structure. The latter may be new structures, for example the conversion of an α-helix into a β-strand, or alternatively the exposure of buried strands upon partial unfolding. These will tend to aggregate to form the cross-β spine described for other systems [27,37–40,53,59]. Similar observations have been reported for SEPT4, suggesting that a similar phenomenon may be at work [27,60]. The results of a WALTZ analysis of all 13 human septins revealed at least one amyloidogenic region within each GTP-binding domain suggesting this to be a general characteristic of the septin family members. Furthermore, one of the two coincident regions given for SEPT2 by both TANGO and WALTZ (that corresponding to the region around residue 150) was also predicted to be amyloidogenic in all 13 human septins. This may indicate a general tendency for all family members to aggregate and it may be worthwhile investigating the possible involvement of different septins in other amyloidogenic conditions. Since this region corresponds to a buried β-strand, significant structural rearrangement would be necessary for it to become directly involved in the formation of the cross-β spine.

Given the physiological role of septins in filament formation, knowledge on their ability to form amyloids is important as it is fundamental to be able to distinguish between these two types of assemblies. Reports of homo-filaments in the literature are scarce [18,25] and their physiological relevance requires further investigation. Interestingly, the diameters of some of the fibers described here for SEPT2 are similar to those previously reported for SEPT4 [27].

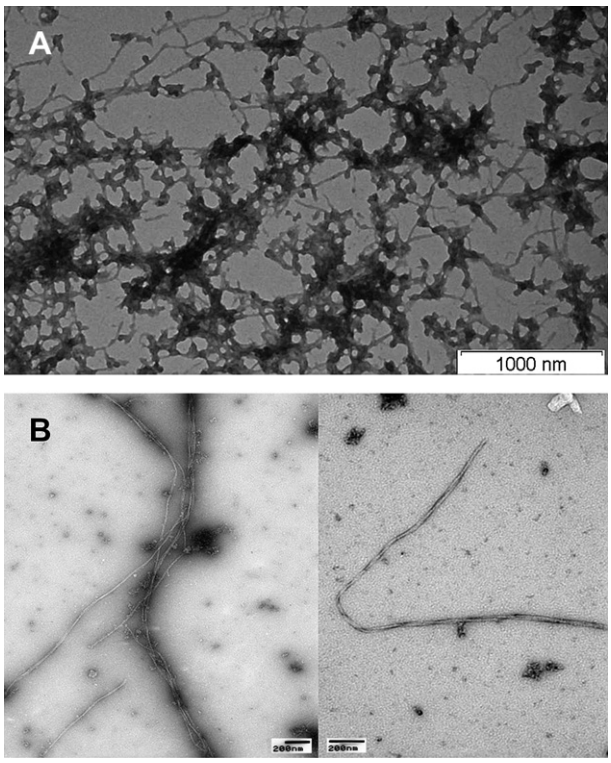

Fig. 7. Electron microscopy. Negatively-stained electron micrograph of SEPT2 fibrils after incubation at: (A) 37 °C for 30 min and (B) 120 h at 4 °C. A scale bar is indicated in each image. The filaments observed in (B) present diameters of 20 nm and lengths up to several micrometers.

4. Conclusions

Septins have been associated with certain neurodegenerative disorders. In particular, SEPT2 has been found to be associated with neurofibrillary tangles and other pathological features of senile plaques in Alzheimer's disease. Since the significance of this finding is unclear, it is important to gain a better understanding of the intrinsic aggregation properties of SEPT2.

In silico prediction programs indicated that the GTP-binding domain of SEPT2 contains regions with a high probability of involvement in aggregation and amyloid formation. This was borne out by experimental data from CD measurements which show a relative loss of α-helical content and a gain in β-sheet structure at around 45 °C, coincident with the tendency to bind the amyloid-specific dye ThT. Although it is not rare for globular proteins to be induced to form amyloid structures *in vitro* under harsh conditions (such as low pHs or high salt concentrations), in the case of SEPT2 and SEPT2G this occurs under near physiological conditions, suggesting that their tendency toward amyloid formation may be relevant to the pathological conditions in which they have been implicated, including Alzheimer's disease.

In summary, these studies should provide a useful basis for future biophysical studies of septin aggregation mechanisms and their role in nervous system disorders. Further studies will be necessary to address whether Septin 2 participates in the development of neurodegenerative diseases or its amyloidosis is a consequence of the underlying pathological processes.

Acknowledgments

We wish to thank Andressa Alves Pinto and Derminda I. de Moraes for technical support. This research was supported by FAPESP via a grant to the Centro de Biotecnologia Molecular e Estrutural.

Appendix. Supplementary data

Supplementary data related to this article can be found online at doi:10.1016/j.biochi.2011.09.014.

References

[1] L.H. Hartwell, Genetic control of the cell division cycle in yeast. IV. Genes controlling bud emergence and cytokinesis, Exp. Cell Res. 69 (1971) 265–276.
[2] M. Kinoshita, The septins, Genome Biol. 4 (2003) 236.
[3] M.C. Surka, C.W. Tsang, W.S. Trimble, The mammalian septin MSF localizes with microtubules and is required for completion of cytokinesis, Mol. Biol. Cell 13 (2002) 3532–3545.
[4] K. Nagata, A. Kawajiri, S. Matsui, M. Takagishi, T. Shiromizu, N. Saitoh, I. Izawa, T. Kiyono, T.J. Itoh, H. Hotani, M. Inagaki, Filament formation of MSF-A, a mammalian septin, in human mammary epithelial cells depends on interactions with microtubules, J. Biol. Chem. 278 (2003) 18538–18543.
[5] S.C. Hsu, C.D. Hazuka, R. Roth, D.L. Foletti, J. Heuser, R.H. Scheller, Subunit composition, protein interactions, and structures of the mammalian brain sec6/8 complex and septin filaments, Neuron 20 (1998) 1111–1122.
[6] E.T. Spiliotis, M. Kinoshita, W.J. Nelson, A mitotic septin scaffold required for mammalian chromosome congression and segregation, Science 307 (2005) 1781–1785.
[7] M. Kinoshita, S. Kumar, A. Mizoguchi, C. Ide, A. Kinoshita, T. Haraguchi, Y. Hiraoka, M. Noda, Nedd5, a mammalian septin, is a novel cytoskeletal component interacting with actin-based structures, Gene Dev. 11 (1997) 1535–1547.
[8] C.L. Beites, H. Xie, R. Bowser, W.S. Trimble, The septin CDCrel-1 binds syntaxin and inhibits exocytosis, Nat. Neurosci. 2 (1999) 434–439.
[9] S. Larisch, Y.S. Yi, R. Lotan, H. Kerner, S. Eimerl, W.T. Parks, Y. Gottfried, S.B. Reffey, M.P. de Caestecker, D. Danielpour, N. Book-Melamed, R. Timberg, C.S. Duckett, R.J. Lechleider, H. Steller, J. Orly, S.J. Kim, A.B. Roberts, A novel mitochondrial septin-like protein, ARTS, mediates apoptosis dependent on its P-loop motif, Nat. Cell Biol. 2 (2000) 915–921.
[10] B.E. Kremer, L.A. Adang, I.G. Macara, Septins regulate actin organization and cell-cycle arrest through nuclear accumulation of NCK mediated by SOCS7, Cell 130 (2007) 837–850.
[11] M. Ihara, A. Kinoshita, S. Yamada, H. Tanaka, A. Tanigaki, A. Kitano, M. Goto, K. Okubo, H. Nishiyama, O. Ogawa, C. Takahashi, O. Ogawa, C. Takahashi, S. Itohara, Y. Nishimune, M. Noda, M. Kinoshita, Cortical organization by the septin cytoskeleton is essential for structural and mechanical integrity of mammalian spermatozoa, Dev. Cell 8 (2005) 343–352.
[12] J.D. Steels, M.R. Estey, C.D. Froese, D. Reynaud, C. Pace-Asciak, W.S. Trimble, Sept12 is a component of the mammalian sperm tail annulus, Cell Motil. Cytoskel 64 (2007) 794–807.
[13] H. Kissel, M.M. Georgescu, S. Larisch, K. Manova, G.R. Hunnicutt, H. Steller, The Sept4 septin locus is required for sperm terminal differentiation in mice, Dev. Cell 8 (2005) 353–364.
[14] B. Kartmann, D. Roth, Novel roles for mammalian septins: from vesicle trafficking to oncogenesis, J. Cell Sci. 114 (2001) 839–844.
[15] J. Zhang, C. Kong, H. Xie, P.S. McPherson, S. Grinstein, W.S. Trimble, Phosphatidylinositol polyphosphate binding to the mammalian septin H5 is modulated by GTP, Curr. Biol. 9 (1999) 1458–1467.
[16] M. Kinoshita, Assembly of mammalian septins, J. Biochem. 134 (2003) 491–496.
[17] S. Hillebrand, W. Garcia, M.D. Cantu, A.P.U. de Araujo, M. Tanaka, T. Tanaka, R.C. Garratt, E. Carrilho, In vitro monitoring of GTPase activity and enzyme kinetics studies using capillary electrophoresis, Anal. Bioanal. Chem. 383 (2005) 92–97.
[18] Y.W. Huang, M.C. Surka, D. Reynaud, C. Pace-Asciak, W.S. Trimble, GTP binding and hydrolysis kinetics of human septin 2, Febs J. 273 (2006) 3248–3260.
[19] C.M. Field, O. AlAwar, J. Rosenblatt, M.L. Wong, B. Alberts, T.J. Mitchison, A purified Drosophila septin complex forms filaments and exhibits GTPase activity, J. Cell Biol. 133 (1996) 605–616.
[20] J.A. Frazier, M.L. Wong, M.S. Longtine, J.R. Pringle, M. Mann, T.J. Mitchison, C. Field, Polymerization of purified yeast septins: evidence that organized filament arrays may not be required for septin function, J. Cell Biol. 143 (1998) 737–749.
[21] C.M. John, R.K. Hite, C.S. Weirich, D.J. Fitzgerald, H. Jawhari, M. Faty, D. Schlapfer, R. Kroschewski, F.K. Winkler, T. Walz, Y. Barral, M.O. Steinmetz, The *Caenorhabditis elegans* septin complex is nonpolar, Embo J. 26 (2007) 3296–3307.
[22] A. Bertin, M.A. McMurray, P. Grob, S.S. Park, G. Garcia, I. Patanwala, H.L. Ng, T. Alber, J. Thorner, E. Nogales, *Saccharomyces cerevisiae* septins: supramolecular organization of heterooligomers and the mechanism of filament assembly, P. Natl. Acad. Sci. USA 105 (2008) 8274–8279.
[23] M. Sirajuddin, M. Farkasovsky, F. Hauer, D. Kuhlmann, I.G. Macara, M. Weyand, H. Stark, A. Wittinghofer, Structural insight into filament formation by mammalian septins, Nature 449 (2007) 311–315.
[24] M. Nakahira, J.N.A. Macedo, T.V. Seraphim, N. Cavalcante, T.A.C.B. Souza, J.C.P. Damalio, L.F. Reyes, E.M. Assmann, M.R. Alborghetti, R.C. Garratt, A.P.U. Araujo, N.I.T. Zanchin, J.A.R.G. Barbosa, J. Kobarg, A draft of the human septin Interactome, Plos One 5 (2010) e0013799.
[25] M. Mendoza, A.A. Hyman, M. Glotzer, GTP binding induces filament assembly of a recombinant septin, Curr. Biol. 12 (2002) 1858–1863.
[26] A.M. Vrabioiu, S.A. Gerber, S.P. Gygi, C.M. Field, T.J. Mitchison, The majority of the *Saccharomyces cerevisiae* septin complexes do not exchange guanine nucleotides, J. Biol. Chem. 279 (2004) 3111–3118.
[27] W. Garcia, A.P.U. de Araujo, F. Lara, D. Foguel, M. Tanaka, T. Tanaka, R.C. Garratt, An intermediate structure in the thermal unfolding of the GTPase domain of human septin 4 (SEPT4/Bradeion-beta) forms amyloid-like filaments in vitro, Biochemistry-US 46 (2007) 11101–11109.
[28] N. Kinoshita, K. Kimura, N. Matsumoto, M. Watanabe, M. Fukaya, C. Ide, Mammalian septin Sept2 modulates the activity of GLAST, a glutamate transporter in astrocytes, Genes Cells 9 (2004) 1–14.
[29] N. Cerveira, C. Correia, S. Bizarro, C. Pinto, S. Lisboa, J.M. Mariz, M. Marques, M.R. Teixeira, SEPT2 is a new fusion partner of MLL in acute myeloid leukemia with t(2; 11)(q37; q23), Oncogene 25 (2006) 6147–6152.
[30] R.A. Craven, S. Hanrahan, N. Totty, P. Harnden, A.J. Stanley, E.R. Maher, A.L. Harris, W.S. Trimble, P.J. Selby, R.E. Banks, Proteomic identification of a role for the von Hippel Lindau tumour suppressor in changes in the expression of mitochondrial proteins and septin 2 in renal cell carcinoma, Proteomics 6 (2006) 3880–3893.
[31] K. Sakai, M. Kurimoto, A. Tsugu, S.L. Hubbard, W.S. Trimble, J.T. Rutka, Expression of Nedd5, a mammalian septin, in human brain tumors, J. Neuro-Oncol. 57 (2002) 169–177.
[32] A.A. Khalil, P. James, Biomarker discovery: a proteomic approach for brain cancer profiling, Cancer Sci. 98 (2007) 201–213.
[33] P. Margutti, M. Sorice, F. Conti, F. Delunardo, M. Racaniello, C. Alessandri, A. Siracusano, R. Rigano, E. Profumo, G. Valesini, E. Ortona, Screening of an endothelial cDNA library identifies the C-terminal region of Nedd5 as a novel autoantigen in systemic lupus erythematosus with psychiatric manifestations, Arthritis Res. Ther. 7 (2005) R896–R903.
[34] A. Kinoshita, M. Kinoshita, H. Akiyama, H. Tomimoto, I. Akiguchi, S. Kumar, M. Noda, J. Kimura, Identification of septins in neurofibrillary tangles in Alzheimer's disease, Am. J. Pathol. 153 (1998) 1551–1560.
[35] D.J. Selkoe, Folding proteins in fatal ways, Nature 426 (2003) 900–904.
[36] P. Westermark, M.D. Benson, J.N. Buxbaum, A.S. Cohen, B. Frangione, S.I. Ikeda, C.L. Masters, G. Merlini, M.J. Saraiva, J.D. Sipe, Amyloid: toward terminology clarification – report from the nomenclature committee of the International society of amyloidosis, Amyloid 12 (2005) 1–4.
[37] F. Chiti, C.M. Dobson, Protein misfolding, functional amyloid, and human disease, Annu. Rev. Biochem. 75 (2006) 333–366.
[38] F. Rousseau, J. Schymkowitz, L. Serrano, Protein aggregation and amyloidosis: confusion of the kinds? Curr. Opin. Struct. Biol. 16 (2006) 118–126.
[39] C.M. Dobson, Principles of protein folding, misfolding and aggregation, Semin. Cell Dev. Biol. 15 (2004) 3–16.
[40] F. Chiti, C.M. Dobson, Amyloid formation by globular proteins under native conditions, Nat. Chem. Biol. 5 (2009) 15–22.
[41] A.M. Fernandez-Escamilla, F. Rousseau, J. Schymkowitz, L. Serrano, Prediction of sequence-dependent and mutational effects on the aggregation of peptides and proteins, Nat. Biotechnol. 22 (2004) 1302–1306.
[42] R. Giraldo, Defined DNA sequences promote the assembly of a bacterial protein into distinct amyloid nanostructures, P. Natl. Acad. Sci. USA 104 (2007) 17388–17393.
[43] S. Maurer-Stroh, M. Debulpaep, N. Kuemmerer, M.L. de la Paz, I.C. Martins, J. Reumers, K.L. Morris, A. Copland, L. Serpell, L. Serrano, J.W.H. Schymkowitz, F. Rousseau, Exploring the sequence determinants of amyloid structure using position-specific scoring matrices, Nat. Methods 7 (2010) 237–U109.
[44] G.G. Tartaglia, M. Vendruscolo, The Zyggregator method for predicting protein aggregation propensities, Chem. Soc. Rev. 37 (2008) 1395–1401.
[45] F. Sanger, S. Nicklen, A.R. Coulson, DNA sequencing with chain-Terminating Inhibitors, P. Natl. Acad. Sci. USA 74 (1977) 5463–5467.
[46] S.C. Gill, P.H. Vonhippel, Calculation of protein Extinction Coefficients from amino-acid sequence data, Anal. Biochem. 182 (1989) 319–326.
[47] H. LeVine 3rd, Thioflavine T interaction with synthetic Alzheimer's disease beta-amyloid peptides: detection of amyloid aggregation in solution, Protein Sci. 2 (1993) 404–410.
[48] H. Naiki, K. Higuchi, M. Hosokawa, T. Takeda, Fluorometric determination of amyloid fibrils in vitro using the fluorescent dye, thioflavin T1, Anal. Biochem. 177 (1989) 244–249.
[49] L.A. Munishkina, A.L. Fink, Fluorescence as a method to reveal structures and membrane-interactions of amyloidogenic proteins, Bba-Biomembranes 1768 (2007) 1862–1885.
[50] M. Lindgren, P. Hammarstrom, Amyloid oligomers: spectroscopic characterization of amyloidogenic protein states, Febs J. 277 (2010) 1380–1388.
[51] J. Reumers, L. Conde, I. Medina, S. Maurer-Stroh, J. Van Durme, J. Dopazo, F. Rousseau, J. Schymkowitz, Joint annotation of coding and non-coding single nucleotide polymorphisms and mutations in the SNPeffect and PupaSuite databases, Nucleic Acids Res. 36 (2008) D825–D829.
[52] W. Garcia, A.P.U. de Araujo, M.D. Neto, M.R.M. Ballestero, I. Polikarpov, M. Tanaka, T. Tanaka, R.C. Garratt, Dissection of a human septin: definition and characterization of distinct domains within human SEPT4, Biochemistry-US 45 (2006) 13918–13931.
[53] R. Nelson, D. Eisenberg, Structural models of amyloid-like fibrils, Adv. Protein Chem. 73 (2006) 235–282.
[54] A.P. Pawar, K.F. Dubay, J. Zurdo, F. Chiti, M. Vendruscolo, C.M. Dobson, Prediction of "aggregation-prone" and "aggregation-susceptible" regions in proteins associated with neurodegenerative diseases, J. Mol. Biol. 350 (2005) 379–392.
[55] R. Linding, J. Schymkowitz, F. Rousseau, F. Diella, L. Serrano, A comparative study of the relationship between protein structure and beta-aggregation in

globular and intrinsically disordered proteins, J. Mol. Biol. 342 (2004) 345–353.
[56] Y. Kallberg, M. Gustafsson, B. Persson, J. Thyberg, J. Johansson, Prediction of amyloid fibril-forming proteins, J. Biol. Chem. 276 (2001) 12945–12950.
[57] G.L. Ellman, A colorimetric method for determining low concentrations of Mercaptans, Arch. Biochem. Biophys. 74 (1958) 443–450.
[58] D. Schomburg, V. Parthiban, M.M. Gromiha, CUPSAT: prediction of protein stability upon point mutations, Nucleic Acids Res. 34 (2006) W239–W242.
[59] J.S. Elam, A.B. Taylor, R. Strange, S. Antonyuk, P.A. Doucette, J.A. Rodriguez, S.S. Hasnain, L.J. Hayward, J.S. Valentine, T.O. Yeates, P.J. Hart, Amyloid-like filaments and water-filled nanotubes formed by SOD1 mutant proteins linked to familial ALS, Nat. Struct. Biol. 10 (2003) 461–467.
[60] W. Garcia, N.C. Rodrigues, M.D. Neto, A.P.U. de Araujo, I. Polikarpov, M. Tanaka, T. Tanaka, R.C. Garratt, The stability and aggregation properties of the GTPase domain from human SEPT4, Bba-Proteins Proteom. 1784 (2008) 1720–1727.